RESEARCH ARTICLE

THOC1 deficiency leads to late-onset nonsyndromic hearing loss through p53-mediated hair cell apoptosis

Luping Zhang[1☉], Yu Gao[1☉], Ru Zhang[2☉], Feifei Sun[1], Cheng Cheng[3], Fuping Qian[1,3], Xuchu Duan[1], Guanyun Wei[1], Cheng Sun[1], Xiuhong Pang[4], Penghui Chen[5,6,7], Renjie Chai[1,3], Tao Yang[5,6,7]*, Hao Wu[5,6,7]*, Dong Liu[1]*

1 Department of Otolaryngology-Head and Neck Surgery, Affiliated Hospital, School of Life Science, Key Laboratory of Neuroregeneration of Jiangsu and Ministry of Education, Co-innovation Center of Neuroregeneration, Nantong University, Nantong, China, 2 Shanghai East Hospital, Department of Otorhinolaryngology Shanghai, Shanghai, China, 3 Key Laboratory for Developmental Genes and Human Disease, Ministry of Education, Institute of Life Sciences, Southeast University, Nanjing, China, 4 Department of Otorhinolaryngology-Head and Neck Surgery, Taizhou People's Hospital, Fifth Affiliated Hospital, Nantong University, Taizhou, China, 5 Department of Otorhinolaryngology-Head and Neck Surgery, Shanghai Ninth People's Hospital, Shanghai Jiaotong University School of Medicine, Shanghai, China, 6 Ear Institute, Shanghai Jiaotong University School of Medicine, Shanghai, China, 7 Shanghai Key Laboratory of Translational Medicine on Ear and Nose Diseases, Shanghai, China

☉ These authors contributed equally to this work.
* yangtfxl@sina.com (TY); wuhao622@sina.cn (HW); liudongtom@gmail.com, tom@ntu.edu.cn (DL)

Abstract

Apoptosis of cochlear hair cells is a key step towards age-related hearing loss. Although numerous genes have been implicated in the genetic causes of late-onset, progressive hearing loss, few show direct links to the proapoptotic process. By genome-wide linkage analysis and whole exome sequencing, we identified a heterozygous p.L183V variant in THOC1 as the probable cause of the late-onset, progressive, non-syndromic hearing loss in a large family with autosomal dominant inheritance. Thoc1, a member of the conserved multisubunit THO/TREX ribonucleoprotein complex, is highly expressed in mouse and zebrafish hair cells. The thoc1 knockout (thoc1 mutant) zebrafish generated by gRNA-Cas9 system lacks the C-startle response, indicative of the hearing dysfunction. Both Thoc1 mutant and knockdown zebrafish have greatly reduced hair cell numbers, while the latter can be rescued by embryonic microinjection of human wild-type THOC1 mRNA but to significantly lesser degree by the c.547C>G mutant mRNA. The Thoc1 deficiency resulted in marked apoptosis in zebrafish hair cells. Consistently, transcriptome sequencing of the mutants showed significantly increased gene expression in the p53-associated signaling pathway. Depletion of p53 or applying the p53 inhibitor Pifithrin-α significantly rescued the hair cell loss in the Thoc1 knockdown zebrafish. Our results suggested that THOC1 deficiency lead to late-onset, progressive hearing loss through p53-mediated hair cell apoptosis. This is to our knowledge the first human disease associated with THOC1 mutations and may shed light on the molecular mechanism underlying the age-related hearing loss.

Author summary

We identified a variant in *THOC1* as the probable cause of the hearing loss in a large family with autosomal dominant inheritance. In addition, we showed THOC1 was expressed in mouse and zebrafish hair cells. Furthermore, we revealed that thoc1 deficiency caused the reduction of hair cell numbers in zebrafish and the hypomorphic Thoc1 induced hair cell apoptosis. These defects could be attenuated by the inhibition of p53.

Introduction

Age-related hearing loss (ARHL) affects over 40% of the population older than 65 years [1]. Based on both human and animal studies, multiple mechanisms have been proposed underlying the development of ARHL. Mitochondrial mutations resulted from accumulative oxidative stress, for example, have long been considered as a major factor for degeneration of hair cells, spiral ganglion cells and acoustic nerve fibers [2, 3]. Recent studies also suggested that loss of cochlear synapses, termed as cochlear synaptopathy, may also contribute to the poor hearing-in-noise for ARHL patients [4, 5]. Nevertheless, apoptosis of the inner ear sensory hair cells, which are nonregenerative in mammals, is a key step towards the ARHL process [6, 7]. In aging CBA/J mice with ARHL, hair cells displayed apoptotic features such as nuclear condensation and have multiple apoptotic pathways activated [8]. Deletion of the pro-apoptotic gene Bak exhibits reduced age-related apoptosis of hair cells and spiral ganglion cells, and a mitochondrially targeted catalase transgene suppresses Bak expression in the cochlea, reduces cochlear cell death, and prevents ARHL [9].

Over the past two decades, more than 40 genes have been identified as the genetic causes of mendelian, late-onset, progressive hearing loss (Hereditary Hearing Loss Homepage, http://hereditaryhearingloss.org/). In addition, a number of genes and loci, including *GRM7* and *IQGAP2* for the former, have been implicated in ARHL by large-scale genome-wide association studies [10–12]. Dysfunction of those genes have been shown to hinder the repair or stability of critical auditory components such as cytoskeleton structure, intercellular junction, fluid homeostasis and synaptic transmission [13]. While such findings provided invaluable resources to gain insights into the molecular basis of the age-related hearing loss, the mechanism underlying the direct cause of the progressive hair cell loss remains elusive. To date, only *TJP2* and *DIABLO*, two genes with link to the apoptosis pathway, have been identified to be associated with dominant, late-onset, progressive hearing loss DFNA51 and DFNA64, respectively [14, 15]. Overexpression of the tight junction protein TJP2 due to a genomic duplication was shown to result in decreased phosphorylation of GSK-3β and altered expression of the apoptosis-related genes, increasing the susceptibility of inner ear cells to apoptosis [15]. A missense p.Ser126Leu mutation in the proapoptotic gene *DIABLO* retained its proapoptotic function but renders the mitochondria susceptible to calcium-induced loss of the membrane potential [14].

THOC1 is an essential member of the conserved THO/TREX ribonucleoprotein (RNP) complex that functions in cotranscriptional recruitment of mRNA export proteins to the nascent transcript [16]. Along with the assembly of other THO/TREX proteins, it has been shown to regulate the coordinated gene expression required for cancer development as well as self-renewal and differentiation of embryonic stem cells [17]. Mice homozygous for the *Thoc1* null allele is embryonic lethal, while those with the *Thoc1* hypomorphic allele exhibited a dwarf phenotype with severely compromised gametogenesis [16, 18, 19]. So far, no pathogenic *THOC1* mutations have been reported to be associated with human disorders and the function

of THOC1 in inner ear has not been explored. In this study, we identified a missense mutation in *THOC1* as the probable cause of late-onset, progressive, non-syndromic hearing loss in a large family with autosomal dominant inheritance. Deficiency of Thoc1 was shown to lead to hair cell apoptosis through the p53-mediated pathway.

Results

Clinical characteristics of Family SH

Family SH had at least 15 members affected by adulthood-onset hearing loss within 4 generations (Fig 1A). The nonsyndromic, bilateral hearing loss was most predominant in the high frequencies, beginning mildly during the fourth decade and gradually progressed to severe-to-profound in the seventh and eighth decades (Fig 1B; S1 Fig). All affected subjects reported tinnitus, while vestibular dysfunction or other clinical abnormalities were not observed. No inner ear malformation was detected by temporal bone computed-tomography (CT) scanning.

Identification of the p.L183V mutation in *THOC1*

Because the onset of the hearing loss was during the fourth decade for Family SH, only unaffected family members over 40 years old were included in the linkage analysis in this study. Multipoint genome-wide linkage analysis of the 9 affected and 12 unaffected family members (marked with asterisks in Fig 1A) detected a 1.57-Mb critical interval on Chromosome 18p11.3 between markers rs4797697 (start of the chromosome) and rs11080868 (Fig 1C; S1 Data). Maximum logarithm of the odds (LOD) score of 4.93 was obtained for markers rs928980, rs1022177 and rs12709528 (S1 Table).

Whole-exome sequencing of four affected (III-4, III-9, III-10 and III-18) and two unaffected (III-16 and IV-6) family members (marked with triangles in Fig 1A) identified a total of three candidate variants (S2 Table). Following Sanger sequencing of all 9 affected and 12 unaffected family members, only the c.547C>G (p. L183V) variant in *THOC1* (NM_005131) segregated with the hearing loss in Family SH (Fig 1D). The coding regions of all genes within the critical interval of the linkage analysis have sequencing depth of 20x or higher. Consistent with the linkage analysis results, the p. L183V variant in *THOC1* is the only candidate pathogenic variant identified within the 1.57-Mb critical interval. Quantitative reversed-transcript PCR detected no significant difference in the relative expression of all 11 protein-coding genes in the critical interval between two family members with (III-10) and without (IV-6) the c.547C>G mutation (S2 Fig).

Since the c.547C>G nucleotide change potentially generates a new donor splice site (CT>GT), we performed reversed-transcript PCR utilizing blood from two family members with (III-10) and without (IV-6) the c.547C>G mutation. No differential mRNA level or alternatively spliced transcript can be detected in the mutant samples (S3 Fig), ruling out the possibility of splicing alternation due to the c.547C>G mutation. Leu183 resides in the elongation factor (efThoc1) domain of THOC1 and is evolutionarily conserved from human to fruit fly (Fig 1E and 1F; S4 Fig). The p.L183V variant was predicted to be pathogenic by computational programs Mutation Taster, PROVEAN and SIFT and was not seen in public databases GnomAD, ExAC, 1000genomes and 1000 Chinese Han normal hearing controls.

The expression of *thoc1* in mouse and zebrafish hair cells

To further elucidate the role of THOC1 in hearing, we investigated the expression of THOC1 in mouse and zebrafish via antibody immunostaining analysis and whole mount *in situ* hybridization using antisense RNA probe. Firstly, we validated the monoclonal Anti-THOC1 antibody using western blot analysis. We demonstrated that Clustered regularly interspaced
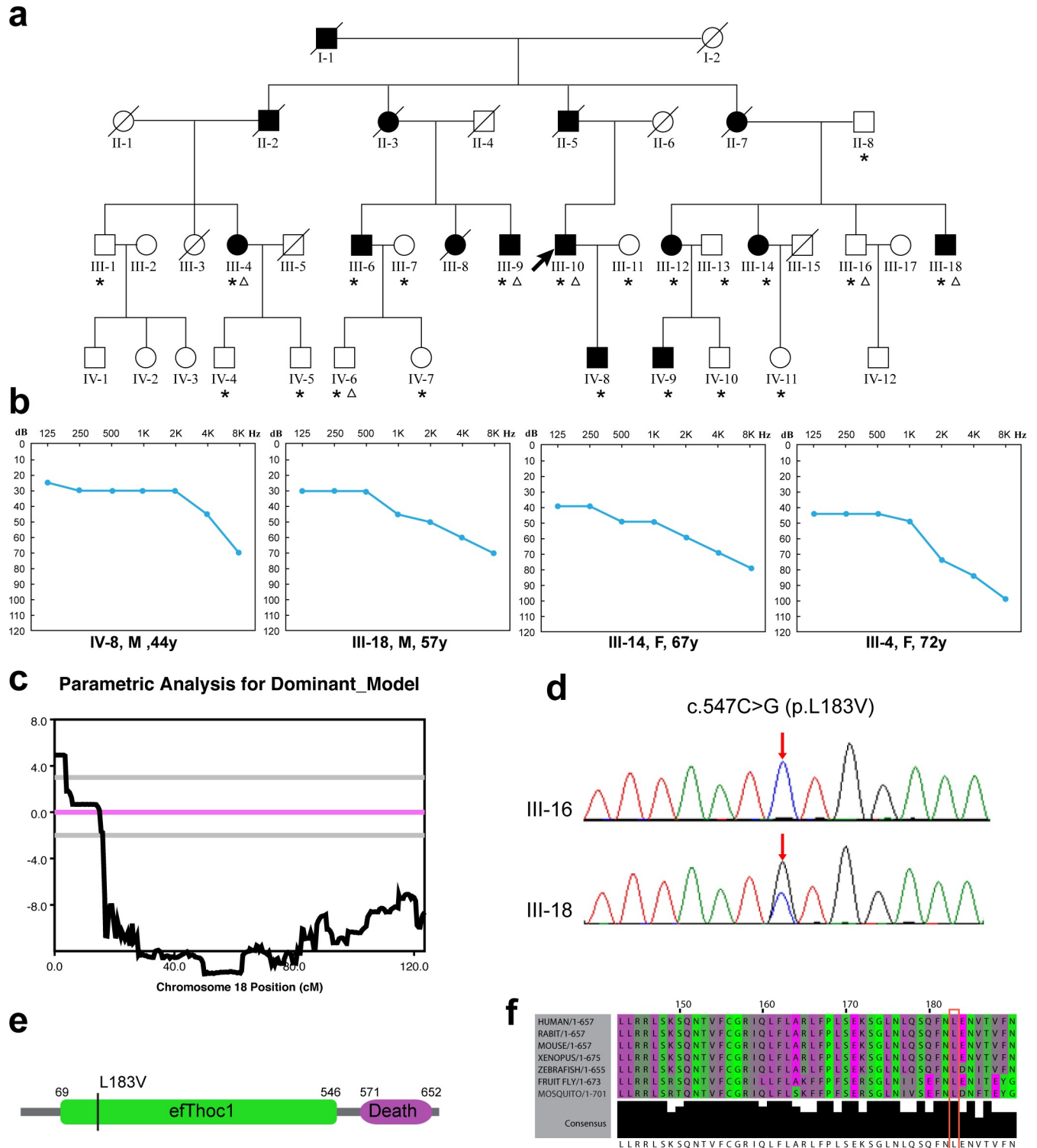
Fig 1. Pedigrees and genotypes of family SH. (a) Pedigrees of family SH. The individuals selected for linkage analysis and whole-exome sequencing was marked with asterisks and triangles, respectively. (b) Representative audiograms of family SH. (c) Logarithm of the odds (LOD) scores of genome-wide linkage analysis for chromosome 18. A maximum LOD score of 4.93 was obtained for marker rs928980. (d) Chromatograms of wild type (WT) and mutant (Mut) sequence for c.547C>G (p.L183V). (e) Diagram showing domains of human THOC1 protein and the location of the p.L183V mutation. (f) Multiple sequence alignment of THOC1 showing conservation of the leucine 183 residue.

short palindromic repeats (CRISPR)/CRISPR-associated protein 9 (Cas9) system mediated Thoc1 knockout resulted in the complete depletion of THOC1 protein in 293t cell (S5A Fig), in which the expression of Thoc1 was relatively high (S5B Fig). These results suggested that the monoclonal Anti-THOC1 antibody was specifically targeting THOC1. Cross-section and immunostaining of P0 mouse inner ear showed that THOC1 was specifically expressed in inner and outer hair cells (Fig 2A and 2B) but not in saccule, utricles, spiral ganglion cells and stria vascularis (S6 Fig). THOC1 protein highly enriched in hair cell nucleus and slightly distributed in cytosol (Fig 2A). Consistently, whole mount *in situ* hybridization in zebrafish showed that *thoc1* was specifically enriched in the zebrafish developing neuromast (Fig 2C–2E').

Thoc1 deficiency caused hair cell developmental defects in zebrafish

In order to examine whether *thoc1* was required for the formation of hair cell, the CRISPR/ Cas9 system was utilized to generate a series of *thoc1* mutants in *Tg(pou4f3:gap43-GFP)* and *Tg (Cldnb:lynGFP)* transgenic zebrafish lines, in which the membrane of hair cell and the neuro-mast epithelium are labeled with GFP respectively [20, 21]. To obtain viable but hypomorphic alleles, we chose the target sites at the exon 20, the second last exon of zebrafish *thoc1* (S7A Fig). The selected gRNA-Cas9 system efficiently induced a series of frameshifting indels in the targeting sites that were predicted to truncating a small portion of the C-terminal protein (S7B Fig). In the following experiments, the red star labeled mutant line was used. In the *thoc1* mutants, the number of hair cells clusters in neuromasts and the number of neuromasts are dramatically decreased (Fig 3A–3D; S8 Fig). Meanwhile, the hair cell number in both each neuromast and in the whole embryo is significantly reduced as well (Fig 3E–3J). Moreover, we found that *thoc1* deficiency caused the reduction of hair cell in the otic vesicles as well (S9 Fig). In addition, we examined the fast escape reflex, the C-shaped startle response. It was found that the probability of the C-startle response in *thoc1* deficient zebrafish was significantly lower than that in control zebrafish embryo and adults, suggesting *thoc1* mutants have hearing problems (S10 Fig, S11 Fig). To verify these phenotypes in *thoc1* mutants were indeed caused by loss of function of *thoc1*, we examined whether *thoc1* knockdown could phenocopy the mutants. A splicing-blocking morpholino (MO) was validated to efficiently interfere the *thoc1* pre-mRNA splicing, caused the exon3 (61 bp) deletion and lead to the reading frame shift (Fig 4A and 4B). Sanger sequencing analysis confirmed this result (S12 Fig). It was demonstrated that *thoc1* morphants had the same phenotypes with those in *thoc1* mutants (Fig 4C). In addition, both human *THOC1* mRNA and zebrafish *thoc1* mRNA significantly rescued the hair cell defects in *thoc1* morphants (Fig 4C and 4D). These results substantiate that hair cell defects were specifically caused by inactivation of *thoc1*.

The p. L183V mutation in *THOC1* impaired its function in hair cell formation

To testify whether the c.547C>G/p.Leu183Val mutation in THOC1 impairs its function in hair cell formation, we explored the effect of this mutation during hair cell development. We setup 6 groups for microinjection and did confocal imaging analysis of hair cells at 4 days post fertilization (dpf): wild-type control, standard MO control, *thoc1*-MO, *thoc1*-MO + *zthoc1* mRNA, *thoc1*-MO + *hTHOC1* mRNA, *thoc1*-MO + *hTHOC1* (c.547C>G) mRNA. We found that microinjection of zebrafish and human mRNA rescued the developmental defects of hair cell caused by inactivation of *thoc1* (Fig 4C and 4D). However, microinjection of *hTHOC1* (c.547C>G) mRNAs into *thoc1* morphants failed to restore the decrease of hair cell number (Fig 4C and 4D). These results suggest the p. L183V mutation in THOC1 impaired its function in hair cell formation.
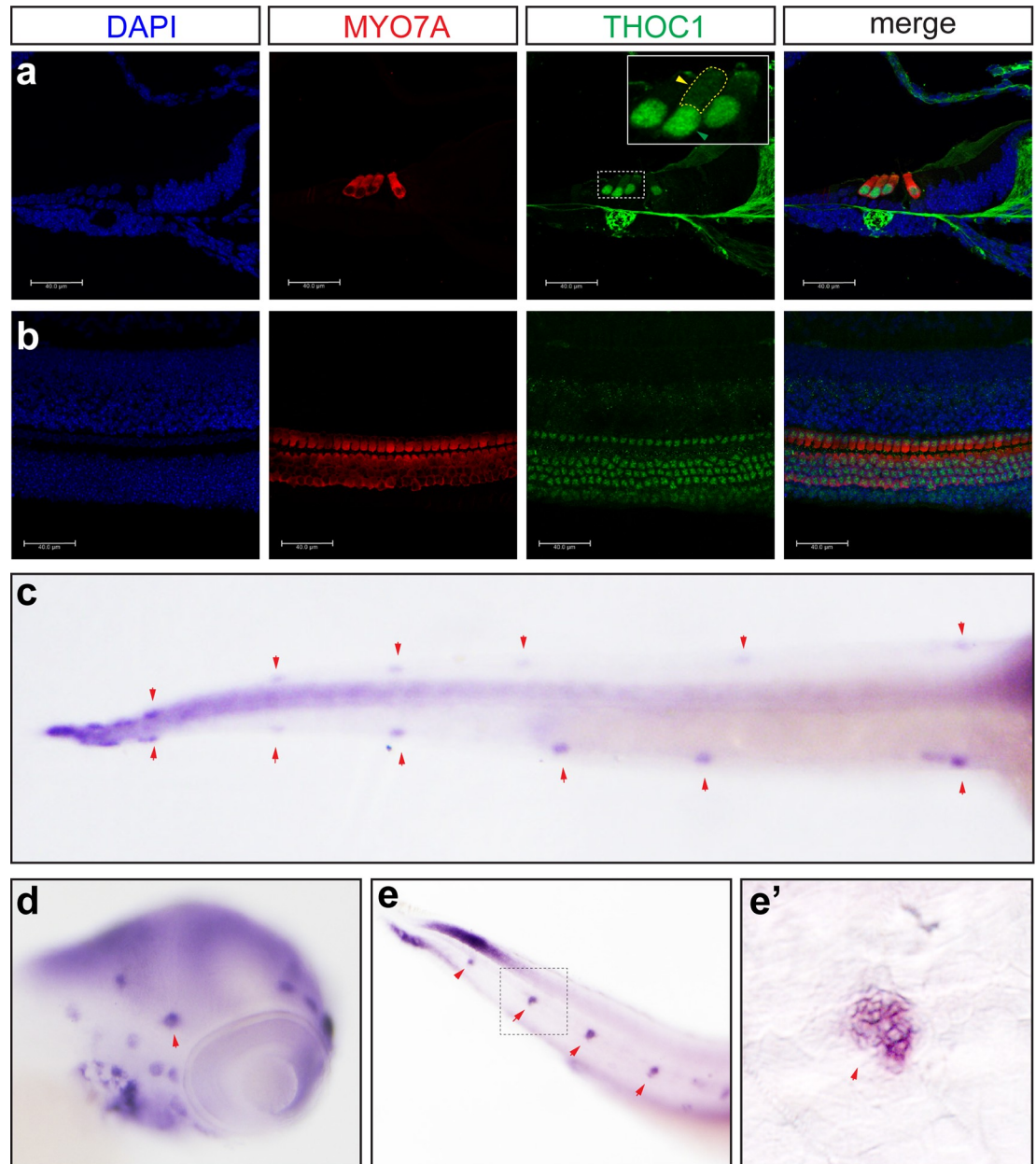
Fig 2. The expression of THOC1 in hair cells. (a, b) Confocal microscopic imaging analysis of THOC1 antibody staining in mouse cochlea hair cells. THOC1 was enriched in outer hair cells (OHC) and inner hair cells (IHC) in the P0 mouse cochlea. Blue: DAPI staining of the cell nuclei. Red: Myosin 7a antibody staining marking hair cells. Green: THOC1 antibody staining. Bars, 40 μm. The region in yellow dash-line rectangle amplified in the white rectangle. Green arrowhead indicates nucleus; yellow arrowhead indicates cytoplasm. (c-e') whole mount *in situ* hybridization analysis of expression of *thoc1* in 3 dpf zebrafish. (c) Dorsal view, arrowheads indicate neuromasts. (d) Lateral view, arrowheads indicate neuromasts. (e) Lateral view, arrowheads indicate neuromasts. (e') Lateral view, arrowheads indicate neuromasts. The magnified region of square in (e).

https://doi.org/10.1371/journal.pgen.1008953.g002

Inactivation of *thoc1* induced apoptosis in neuromasts

To understand the cellular mechanism by which the hair cells were dramatically decreased, we did the confocal imaging analysis of the residual cells. In *thoc1* mutants, we found that around 83% of these hair cells had an abnormal morphology, such as distorted shape, quite smaller,
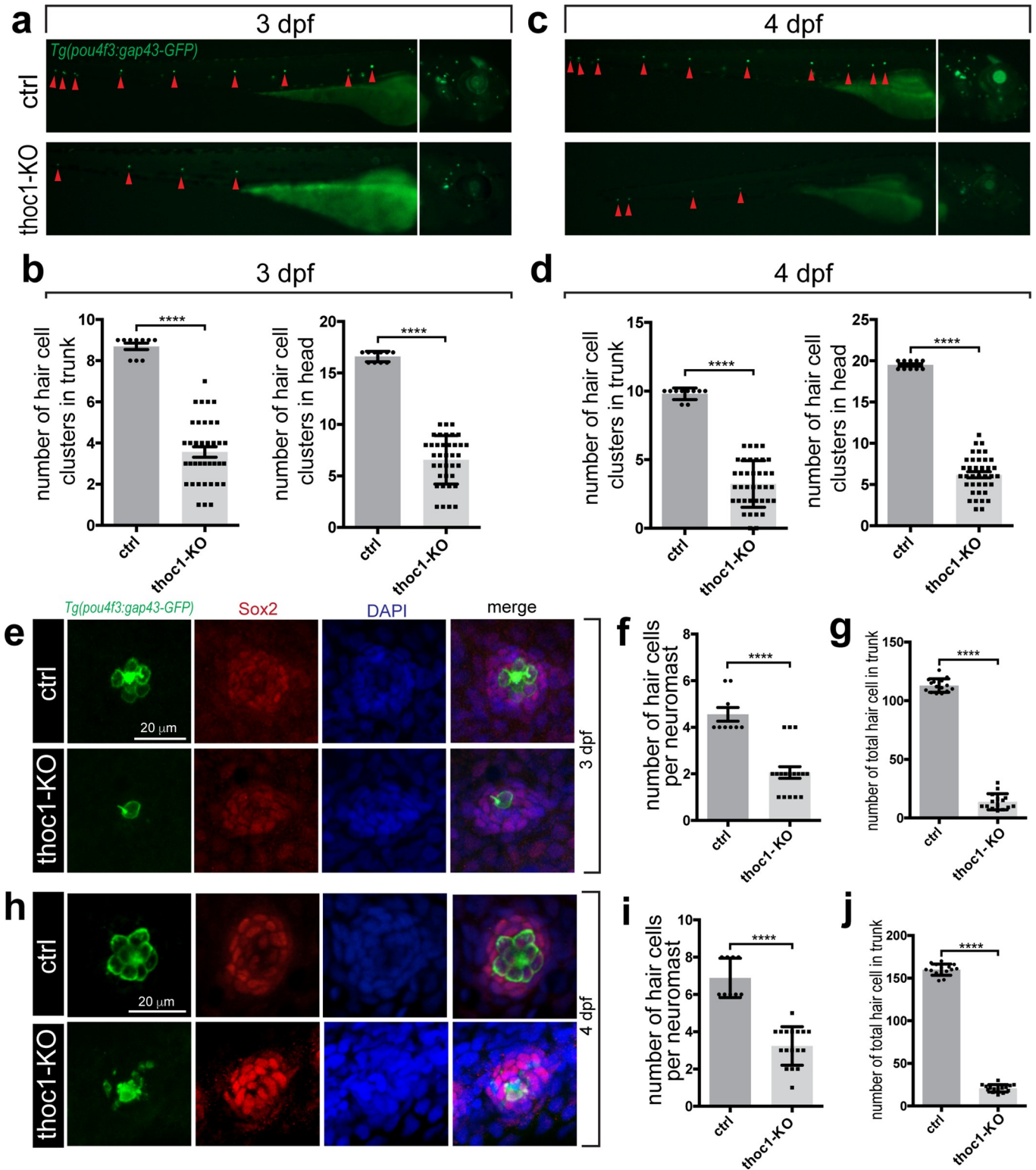
Fig 3. *Thoc1* deficiency caused hair cell developmental defects in zebrafish. (a) Fluorescence microscopic imaging analysis of *thoc1* mutant *Tg(pou4f3: gap43-GFP)* line at 3 dpf. Arrowheads indicate hair cell clusters. (b) Statistical analysis of the hair cell clusters in control and *thoc1* mutants (control, n = 10; *thoc1* mutants, n = 37). *t*-test, ****, *p*<0.0001. (c) Fluorescence microscopic imaging analysis of *thoc1* mutant *Tg(pou4f3:gap43-GFP)* line at 4 dpf. Arrowheads indicate hair cell clusters. (d) Statistical analysis of the hair cell clusters in control and *thoc1* mutants (control, n = 10; *thoc1* mutants, n = 38). *t*-test, ****, *p*<0.0001. (e) Confocal microscopic imaging analysis of the neuromasts in control and *thoc1* mutants at 3 dpf. Green: *Tg(pou4f3:gap43-GFP)*. Red: Sox2

antibody staining marking supporting cells. Blue: DAPI staining of the cell nuclei. (f, g) Statistical analysis of the hair cell number per neuromasts and total number in trunk of control and *thoc1* mutants (control, n = 9; *thoc1* mutants, n = 17, control, n = 15; *thoc1* mutants, n = 15) at 3 dpf. *t*-test, ****, *p*<0.0001. (h) Confocal microscopic imaging analysis of the neuromasts in control and *thoc1* mutants at 4 dpf. Green: *Tg(pou4f3:gap43-GFP)*. Red: Sox2 antibody staining marking supporting cells. Blue: DAPI staining of the cell nuclei. (i, j) Statistical analysis of the hair cell number per neuromasts and total number in trunk of control and *thoc1* mutants (control, n = 9, *thoc1* mutants, n = 17; control, n = 15; *thoc1* mutants, n = 15) at 4 dpf. *t*-test, ****, *p*<0.0001.

and even became cell fractions (Fig 5A). These results suggest a number of hair cells underwent apoptosis. To test this hypothesis, we carried out Terminal deoxynucleotidyl transferase dUTP nick end labeling (TUNEL) analysis, which is a method for detecting apoptotic DNA fragmentation [22, 23], in *thoc1* mutants. It was revealed that *thoc1* deficiency resulted in 45% hair cell and supporting cell apoptosis in neuromasts (Fig 5B).

In addition, we performed the transcriptome sequencing analysis of the *thoc1* mutated embryos at 48 hpf. We found that 455 genes were significantly up-regulated, while 1312 genes were significantly down-regulated in *thoc1* mutants compared to the sibling control (Fig 6A and 6B). Kyoto Encyclopedia of Genes and Genomes (KEGG) [24] pathway analysis of these
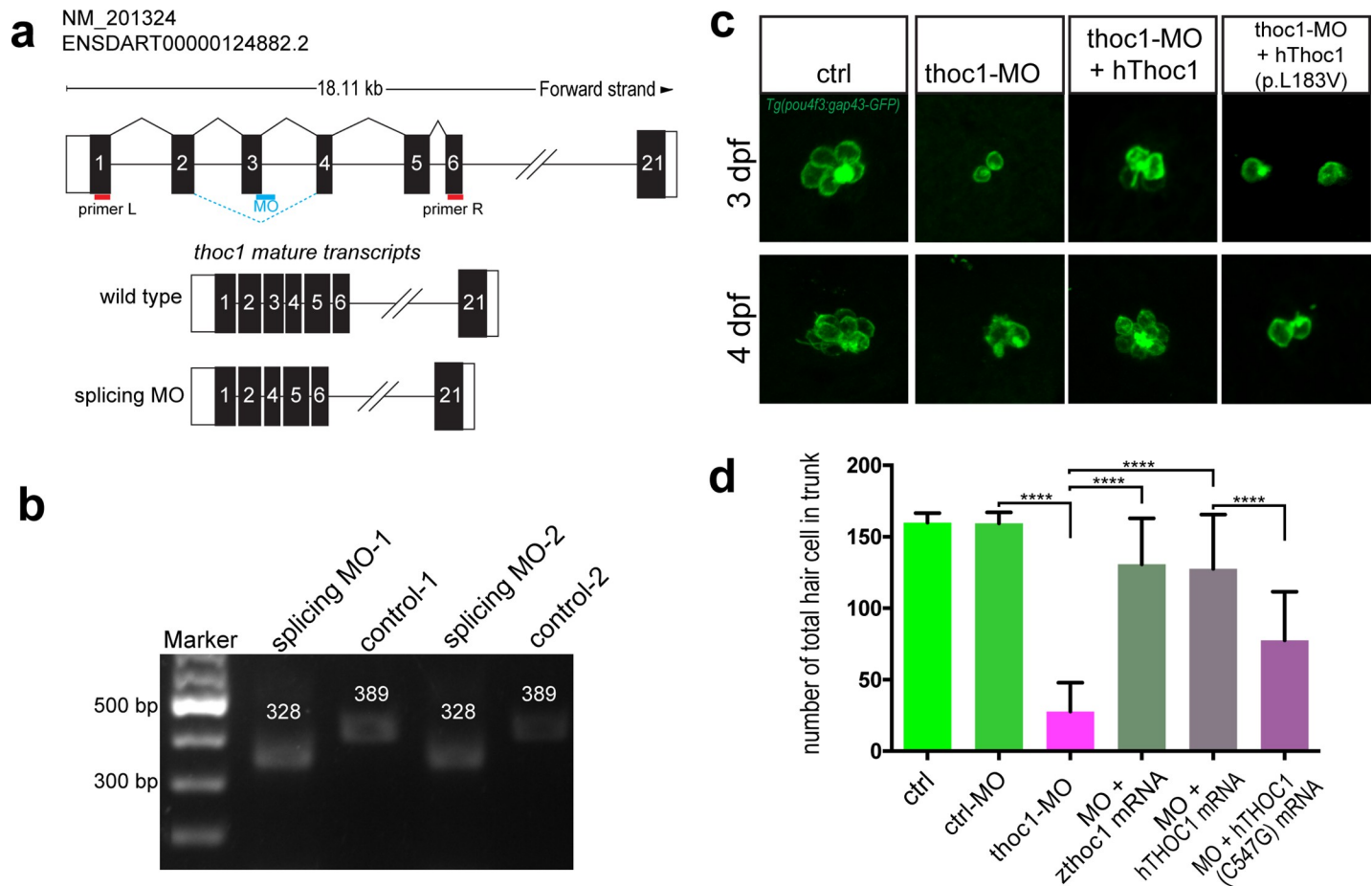
Fig 4. The THOC1 mutation (p. L183V) impaired its function in hair cell formation. (a) The diagram shows the targeting site of *thoc1* splice blocking morpholino and the RT-PCR primers design for validating the knockdown results. The wild type mature transcripts indicate the natural splicing product of *thoc1* mRNA. The splicing MO mature transcripts indicate the abnormal splicing product of *thoc1*mRNA with Exon3 deletion caused by morpholino injection. (b) The agarose gel electrophoresis image shows the 61bp Exon3 deletion. (c) Confocal microscopic imaging analysis of the hair cells in control, *thoc1*-MO, *thoc1* -MO + *hThoc1* mRNA, and *thoc1*-MO + *hThoc1* (p. L183V) mRNA *Tg(pou4f3:gap43-GFP)* at 3 dpf and 4 dpf. (d) Statistical analysis of the total hair cell number in trunk of control (n = 15), control-MO (n = 15), *thoc1*-MO (n = 15), *thoc1*-MO + *zthoc1* mRNA (n = 15), *thoc1*-MO + *hThoc1* mRNA (n = 15), and *thoc1*-MO + *hThoc1* (p. L183V) mRNA at 4 dpf (n = 15). One-way ANOVA, ****, *p*<0.0001.

Fig 5. Inactivation of *thoc1* induced apoptosis in neuromasts. (a) Confocal microscopic imaging analysis of the hair cells in control and *tho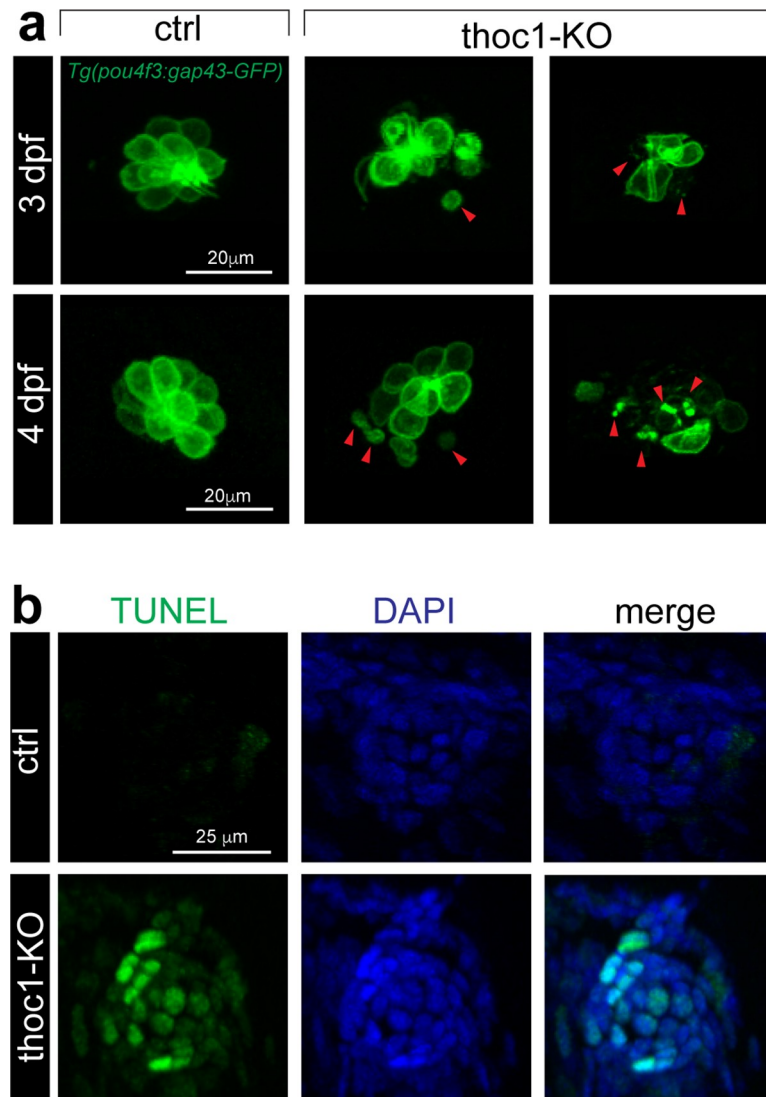c1*-KO *Tg(pou4f3:gap43-GFP)* at 3 and 4 dpf. Arrowheads indicate the abnormal hair cells. (b) TUNEL analysis of the neuromasts in control and *thoc1*-KO embryos at 4 dpf. Green: TUNEL staining. Blue: DAPI staining of the cell nuclei.

https://doi.org/10.1371/journal.pgen.1008953.g005

different expression genes revealed that 35 pathways were enriched, including P53 signaling pathway, which can promote apoptosis [25], DNA replication, and cell cycle (Fig 6C). The *p53* upregulation was validated by Realtime PCR analysis at 48 hpf and 72 hpf (Fig 6D). In addition, Realtime PCR analysis indicated that apoptosis genes *bax* [26], *casp3* [27] and *casp9* [28] were significantly up-regulated in 4 dpf *thoc1* mutants (Fig 6E). These results were in support of that inactivation of *thoc1* induced apoptosis in neuromasts.

To confirm the hair cell reduction in *thoc1* deficient embryos was due to the cell apoptosis, we knockdown the *thoc1* in *p53* mutated zebrafish embryos and did the vital dye FM1-43FX staining to visualize and image the hair cells in lateral line neuromasts. It was revealed that depletion of *p53* partially normalized the number of hair cells in *thoc1* morphants (S13 Fig). Additionally, treatment of 5 µM Pifithrin-α, which is an inhibitor of p53, treatment in the *thoc1* mutants from 3 dpf to 4 dpf significantly restored the reduction of the number of hair
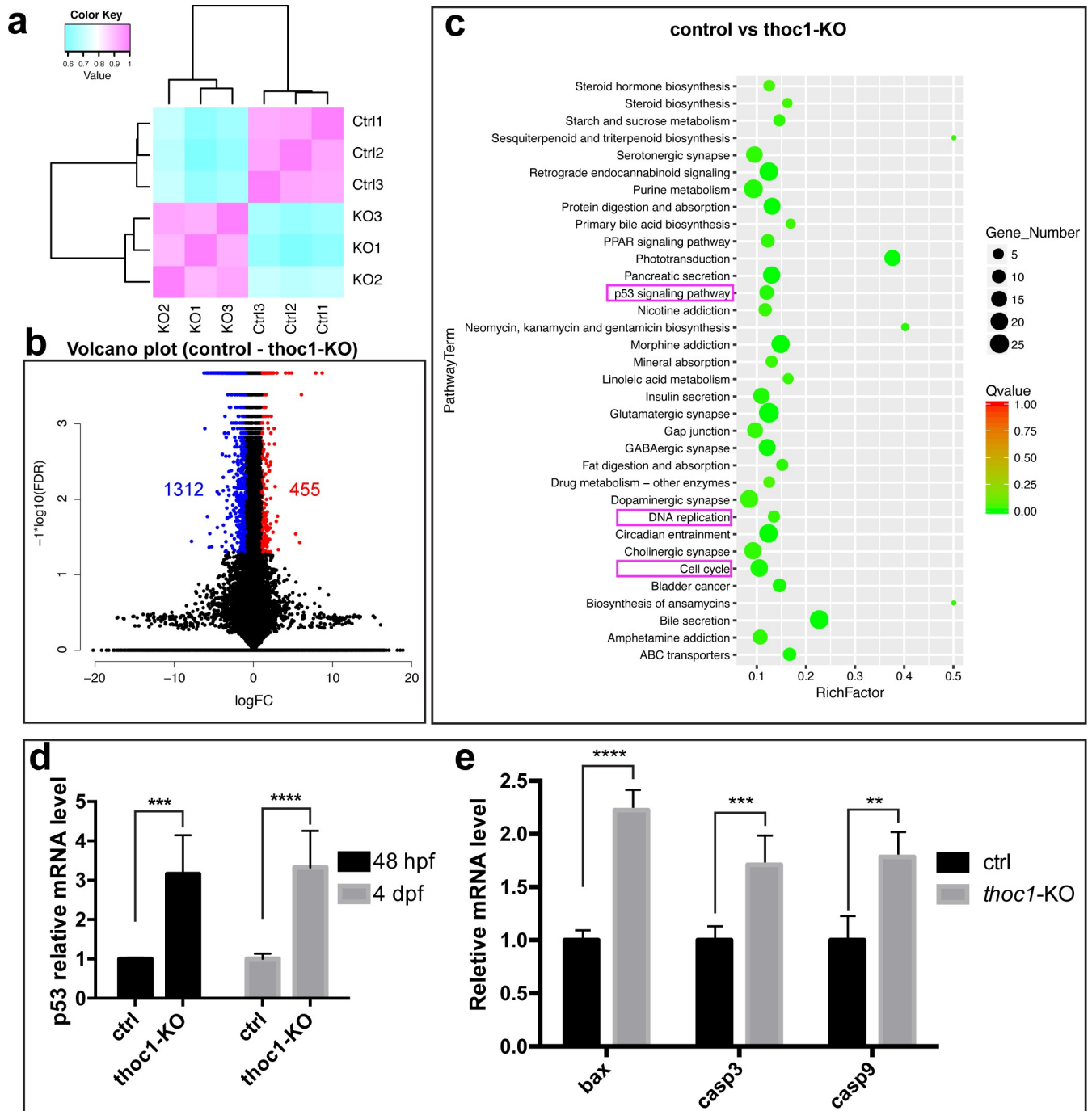
Fig 6. Transcriptome sequencing analysis of 48 hpf *thoc1* mutants. (a) Clustering analysis indicates the replicates within group have a good repeatability, while the control and mutated group are different. (b) Volcano diagram of different expression genes. Red dots indicate up-regulated genes; blue dots indicate down-regulated genes. Abscissa indicates gene fold change in different samples; ordinate represents statistical significance of gene expression change. (c) KEGG analysis plot of the differential gene, with the vertical axis representing the pathway and the horizontal axis representing the Rich factor. The size of the dot indicates the number of differentially expressed genes in the pathway, and the color of the dot corresponds to a different Qvalue range. (d) Relative mRNA levels of *p53* in control and *thoc1*-KO embryos at 48 hpf and 4 dpf (three times experiments, n = 10 for each time). *t*-test; [***], $p<0.001$; [****], $p<0.0001$. (e) Relative mRNA levels of *bax*, *casp3* and *casp9* in control and *thoc1*-KO embryos at 4 dpf (three times experiments, n = 10 for each time), *t*-test; [**], $p<0.01$; [***], $p<0.001$; [****], $p<0.0001$.
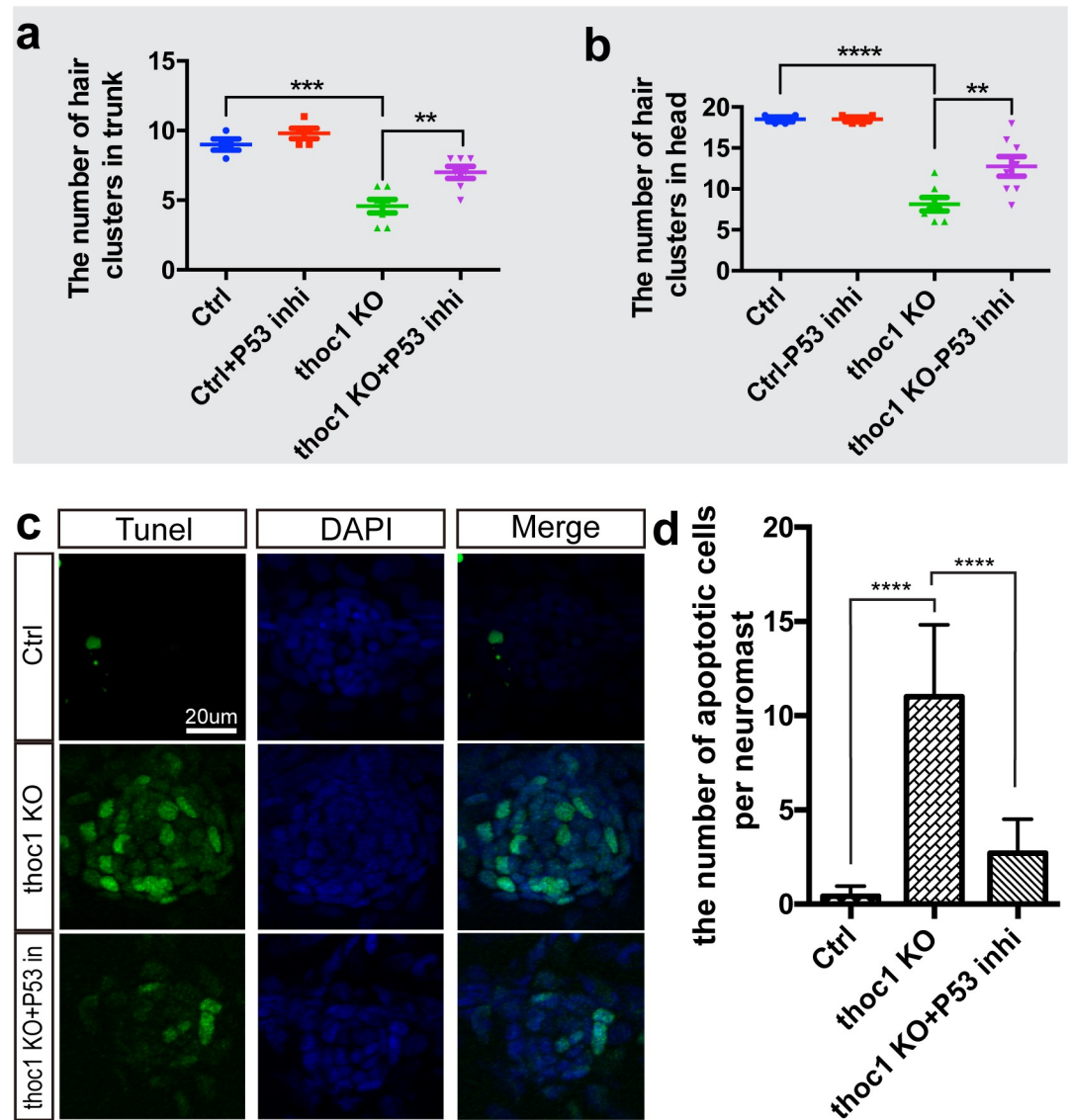
Fig 7. Inhibition of P53 signaling alleviated the *thoc1*-deficiency induced apoptosis in neuromasts. (a, b) Statistical analysis of the hair cell clusters in control (n = 8), ctrl + P53 inhibitor treatment (n = 9), *thoc1* KO (n = 8), and *thoc1* KO + P53 inhibitor treatment embryos (n = 7). One-way ANOVA, ****, $p<0.0001$; ***, $p<0.001$; **, $p<0.01$. (c) TUNEL analysis of the neuromasts in control (n = 7), *thoc1* KO (n = 7), and *thoc1* KO + P53 inhibitor treatment embryos (n = 7). Green: TUNEL staining. Blue: DAPI staining of the cell nuclei. (d) Statistical analysis of the number of apoptotic cells per neuromast in control, *thoc1* KO, and *thoc1* KO + P53 inhibitor treatment embryos. One-way ANOVA, ****, $p<0.0001$.

cell clusters (Fig 7A and 7B; S14 Fig). Furthermore, we found that the Pifithrin-α treatment significantly alleviated *thoc1*-deficien*y* induced apoptosis in neuromasts using TUNEL analysis (Fig 7C and 7D)

Discussion

As a key component of the TREX protein complex, THOC1 is evolutionarily conserved and plays an essential role for coordinated gene expression during early and postnatal development [16, 18, 19]. In humans, non-synonymous variants in *THOC1* are extremely rare, as no such

variants have minor allele frequencies higher than 0.002 in the Genome Aggregation Database (gnomAD, http://gnomad.broadinstitute.org/). In this study, we presented to our knowledge the first *THOC1* mutation associated with human mendelian disorders. Several lines of genetic and functional evidences supported that the p.L183V variant in *THOC1* is the probable cause of the late-onset, non-syndromic hearing loss in Family SH: a) *THOC1* was harbored in the 1.57-Mb critical interval defined by genome-wide linkage analysis with a very high maximum LOD score of 4.93; b) Exome sequencing identified p.L183V in *THOC1* as the only candidate pathogenic variant segregating with the hearing phenotype in 21 members of Family SH; c) the p.L183V variant changed a highly conserved amino acid, was predicted to be pathogenic by computational programs Mutation Taster, PROVEAN and SIFT, and was not seen in public databases GnomAD, ExAC, 1000genomes and 1000 ethnically matched normal hearing controls; d) the hair cell loss of the *thoc1*-knockdown zebrafish can be functionally rescued by embryonic microinjection of the wild-type *thoc1* mRNA, but to significantly lesser degree by that of the p.L183V mutant mRNA.

Even though THOC1 regulates expression of a wide range of genes required for crucial biological processes such as embryogenesis, organogenesis and cellular differentiation [17], mice with hypomorphic alleles in *Thoc1* were viable [19] and are associated with tissue-specific defects such as compromised fertility [18]. In our study, the affected members of Family SH showed no abnormalities other than the hearing loss, further demonstrating that systematic reduced level of functional Thoc1 is generally tolerated and may lead to certain tissue-restricted disorders.

To elucidate the role of THOC1 in the inner ear, we generated a series of *Thoc1* mutant zebrafish that mimicked the human hearing impairment by losing the C-startle response. These mutants likely represented hypomorphic alleles of *Thoc1* as the MO-knockdown zebrafish had similar phenotype. In inner ear, the most striking finding from both *Thoc1* mutant and knock-down zebrafish is the marked loss of hair cells due to apoptosis. Surprisingly, though hair cell apoptosis is a key step towards progressive and age-related hearing loss, *THOC1* represents only one of a very few deafness-causing genes directly involved in this process. Given THOC1 regulates distinct and specific sets of downstream genes in different tissues and development stages, the *Thoc1* deficiency zebrafish generated in our study presented a good model to study the coordinated control of hair cell apoptosis at the molecular level. Indeed, by transcriptome sequencing, we identified a list of genes that were differentially expressed in the *Thoc1* mutant zebrafish. Among them, genes in pathways associated with apoptosis such as p53 signaling, DNA replication and cell cycle were enriched.

Previous studies have suggested dual roles of Thoc1 in relation to cell proliferation and apoptosis depending on the context of different tissues and cell types. In embryonic development of *Rb1* null mice, Thoc1 is required to for increasing expression of *E2f* and other apoptotic regulatory genes [29]. On the other hand, Thoc1 is overexpressed in a variety of cancers [30, 31], and depletion of Thoc1 in those cancer cells, but not in normal cells, induce apoptotic cell death [32]. In mouse models, hypomorphic *Thoc1* allele lead to germ cell apoptosis that in testes correlates with the decreased number of primary spermatocytes [18]. In consistence with the latter findings, our study demonstrated that Thoc1 deficiency may induce hair cell apoptosis in zebrafish, which likely underlies the pathogenic mechanism of the late-onset, progressive hearing loss in Family SH. As a limitation of this study using the zebrafish model for functional characterization of *Thoc1* deficiency, we cannot recapture the late-onset, progressive hearing loss phenotype as shown in human patients. A mouse model should be required to address this issue in future studies. Nevertheless, our study did show that accompanied with the Thoc1 deficiency was the increased expression of a number of downstream apoptotic genes such as *P53*, *Bax*, *Casp3* and *Casp9*. The p53 signaling pathway has been implicated in the hair cell

apoptosis during age-related hearing loss [33]. In our study, we showed that inhibition of P53 by Pifithrin-α significantly alleviated the hair cell apoptosis in the *Thoc1* MO-knockdown zebrafish, presenting a potential new strategy for preventing of the age-related hearing loss.

In conclusion, our study identified *THOC1* as a new possible causative gene for late-onset, progressive hearing loss in humans. Functional studies showed that Thoc1 deficiency unleashes expression of proapoptotic genes in the p53 signaling pathway and results in hair cell apoptosis in zebrafish. These findings may provide important insight into the molecular basis of age-related hearing loss.

Materials and methods

Ethics statement

The study of Hearing Loss on Family SH has been approved by the ethics committee of Affiliated Hospital of Nantong University, Nantong, China (the approval number: 2018-L096). Prior to the studying, the written informed consent from each individual were obtained, according to the guidelines of the ethics committee of Affiliated Hospital of Nantong University. The zebrafish and mouse study were conducted conforming to the local laws and the Chinese law for the Protection of Animals. The mouse experiments were ethically approved by the Administration Committee of Experimental Animals, Jiangsu Province, China [Approval ID: 20180803–034].

Subjects and clinical evaluation

Members of Family SH was recruited through the Affiliated Hospital of Nantong University in Nantong, Jiangsu Province, China. A total of 9 affected and 18 unaffected members participated in the present study (Fig 1A, asterisks). All subjects received comprehensive auditory evaluation including pure tone audiometry (PTA), otoscopic examination and temporal bone high-resolution CT scanning. Family history and general physical examination were performed to exclude the possible syndromic hearing loss.

Genome-wide linkage analysis

Genome-wide multipoint linkage analysis was performed using the HumanOmniZhongHua-8 BeadChip (Illumina, San Diego, USA) and based on genotypes of 6301 Tag SNPs with an averaged 0.5cM resolution. Logarithm of the odds (LOD) scores were calculated by the parametric linkage analysis package Merlin v. 1.1.23. The inheritance model was set to dominant with full penetrance. The disease allele frequency was set to 0.0001.

Whole-exome sequencing and verification of the pathogenic variants

Whole-exome sequencing was performed in four affected (III-4, III-9, III-10 and III-18) and two unaffected (III-16 and IV-6) members (marked with triangles in Fig 1A). Exons and flanking intronic regions of 20794 genes (33.2 Mb, 97.2% of cCDS coding exons), microRNAs and other non-coding RNAs were captured by Illumina TruSeq Exome Enrichment Kit and sequenced on a HiSeq 2000 instrument (Illumina, San Diego, CA, USA). Reads were aligned to NCBI37/hg19 assembly using the BWA Multi-Vision software package. SNPs and indels were identified using the SOAPsnp software and the GATK Indel Genotyper, respectively. Candidate pathogenic variants were defined as nonsense, missense, splice-site and indel variants with allele frequencies of 0.001 or less in public variant databases dbSNP, 1000 Genomes and previous sequencing data of 1000 Chinese Han adult normal hearing controls (in-house whole-exome sequencing data using the same platform). Candidate pathogenic variants were

further genotyped in all family members by Sanger sequencing. Possible pathogenic effects of the identified mutation were evaluated by computational tools including Mutation Taster (http://www.mutationtaster.org), PROVEAN and SIFT (with cut-off scores set at -1.3 and 0.05, respectively, http://sift.jcvi.org).

Immunostaining of THOC1 in mouse inner ear

Immunofluorescence staining of THOC1 was performed in cross-section and whole mount samples of mouse inner ear as previously described [34]. All procedures of the present study had approval from the Animal Use and Care Committee of Affiliated Hospital of Nantong University. Antibodies used in this study included mouse anti-THOC1 (SAB2702154, Sigma-Aldrich, St. Louis, MO), rabbit anti-MYOSIN VIIA (25–6790, Proteus Biosciences, Ramona, CA), and DAPI (D3571, Thermo-fisher, Waltham, MA). Immunostaining presented in figures was representative of two individual experiments.

Zebrafish Line and Startle Response Test

The zebrafish embryos and adults were maintained in zebrafish Center of Nantong University under standard conditions in accordance with our previous procedures [35, 36]. The transgenic zebrafish lines *Tg(pou4f3:gap43-GFP)* and *Tg(cldnb:lynGFP)* were used as previously described [21]. Sound-evoked C-shaped startle response was tested at larval and adult stage in a well-plate and a plastic tank and recorded with a high-speed camera.

RNA Isolation, Reverse Transcription (RT) and Realtime PCR

Total RNA was extracted from zebrafish embryos by TRIzol reagent according to the manufacturer's instructions (Thermo Fisher Scientific, USA). Genomic contaminations were removed by DNaseI, and then 2 µg total RNA was reversely transcribed using a reversed first strand cDNA synthesis kit (Fermentas, USA) and stored at −20˚C. The sequences of PCR primers, used for validating the Splice-blocking Morpholino, were: 5'-TCCGTCTCACTTCGACTTC A-3' and 5'-TCCCAGCAGAGTAAAATGTGT-3'. The Realtime PCR analysis was performed according to the procedure described in our previous work [35]. The primers were used for the *bax*: 5'-AGAGGGTGAAACAGACCAGC-3' and 5'-GCTGAACAAGAAAGGGCACA G-3'; for *caspase3*: 5'-TGGCACTGACGTAGATGCAG-3' and 5'- GAAAAACACCCCCTC ATCGC-3'; for *caspase9*: 5'-ACTAAATGACCGCAAGGGCT-3' and 5'-TTGCCTCAGTGC CATGTGAA-3'; for *p53*: 5'-GCAAAAACTTGCCCCGTTCA-3' and 5'-GCTGATTGCCCT CCACTCTT-3'.

Whole mount *in situ* hybridization

A 498 bp cDNA fragment of Thoc1 was amplified from the cDNA library that established from wild type (WT) AB embryos using the specific primers of *thoc1* F1 5'-TGGAATCTGAA CCCCGACAA-3' and *thoc1* R1 5'-TGTCCGACTCGATCACTCTG-3'. Digoxigenin-labeled sense and antisense probes were synthesized using linearized pGEM-Teasy vector subcloned with this *thoc1* fragment by *in vitro* transcription with DIG-RNA labeling Kit (Roche, Switzerland). Zebrafish embryos and larvae were collected and fixed with 4% paraformaldehyde (PFA) in phosphate-buffered saline (PBS) for one night. The fixed samples were then dehydrated through a series of increasing concentrations of methanol and stored at −20˚C in 100% methanol eventually. Whole mount *in situ* hybridization was subsequently performed as described in the previous study [37, 38].

sgRNA/ Cas9 mRNA synthesis and injection

Cas9 mRNA was obtained by in vitro transcription with the linearized plasmid pXT7-Cas9 according to the procedure previously described. The sgRNAs were transcribed from the DNA templates that amplified by PCR with a pT7 plasmid as the template, a specific forward primer and a universal reverse primer. The gRNA sequence is listed in the following: 5'-TAATACGA CTCACTATAGGTGATTAAAACCGGAGAGGGTTTTAGAGCTAGAAATAGC-3'. *Cas9* mRNAs were synthesized *in vitro* using the linearized constructs as templates with SP6/T7 mMESSAGE mMACHINE Kit (Thermo Fisher Scientific, USA), purified with RNeasy Mini Kit (Qiagen, Germany), and dissolved in RNase free Ultrapure water (Thermo Fisher Scientific, USA). The sgRNAs were synthesized by the MAXIscript T7 Kit (Thermo Fisher Scientific, USA), and were purified with RNeasy Mini Kit (Qiagen, Germany), and dissolved in RNase free Ultrapure water (Thermo Fisher Scientific, USA). Zebrafish lines were naturally mated to obtain embryos for microinjection. One to two-cell stage zebrafish embryos was injected with 2–3 nl of a solution containing 250 ng/μl *Cas9* mRNA and 15 ng/μl sgRNA. At 24 h post fertilization (hpf), zebrafish embryos were randomly sampled for genomic DNA extraction according to the previous methods to determine the indel mutations by sequencing.

Morpholino and mRNAs injections

Thoc1 splice-blocking Morpholino (MOs; Gene Tools, USA) sequence was 5′- AGTAAGCTG TGGACTCACTATCTGC -3′. The sequence of a standard control MO oligo was 5′-CCTCT TACCTCAGTTACAATTTATA-3′. The MOs were diluted to 0.3 mM with RNase-free water and injected into the yolk of one to two-cell stage embryos and then raised in E3 medium at 28.5˚C. The cDNAs containing the open reading frame of the target genes were cloned into PCS2+ vector respectively and then was transcribed *in vitro* using the mMESSAGE mMA-CHIN Kit (Thermo Fisher Scientific, USA) after the recombinant plasmids linearized with NotI Restriction Enzyme (NEB, USA), and then the capped mRNAs were purified by RNeasy Mini Kit (Qiagen, Germany). 2 nl target genes mRNA were injected at 50 ng/μl into 1/2-cell stage embryos.

FM1-43FX labeling and small molecule treatment

To visualize and image the hair cells in lateral line neuromasts, the vital dye FM1-43FX (Thermo Fisher Scientific, USA) was applied at a concentration of 3 μM to live larvae for 45 s in the dark. After quickly rinsing three times with fresh water, the larvae were anesthetized in 0.02% MS-222 and fixed with 4% PFA in PBS for 2 h at room temperature or overnight at 4˚C. 5 μM Pifithrin-α (P4359, Sigma-Aldrich) were diluted in the E3 solution. The embryos were treated from 3 dpf.

TUNEL staining

For TUNEL (Terminal deoxynucleotidyl transferase-mediated dUTP nick end labeling) assays, larvae were incubated in 0.1 M glycine/PBS solution for 10 min and then rinsed with PBT-2 three times for 10 minutes each. The larvae were then processed using the *In Situ* Cell Death Detection Kit (Roche, Switzerland) following the directions supplied by the manufacturer.

mRNA sequencing by Illumina HiSeq

Total RNA of each sample was extracted using TRIzol Reagent (Invitrogen). RNA samples were quantified and qualified by Agilent 2100 Bioanalyzer (Agilent Technologies, USA). Next generation sequencing library preparations were constructed according to the manufacturer's

protocol (Illumina, USA). The libraries were sequenced using Illumina HiSeq instrument according to manufacturer's instructions (Illumina, USA). The sequences were processed and analyzed by GENEWIZ. Differential expression analysis was carried out using the DESeq Bioconductor package. After adjusted by Benjamini and Hochberg's approach for controlling the false discovery rate, P-value of genes were set <0.05 to detect differential expressed ones.

Microscopy and statistical analysis

Zebrafish embryos were anesthetized with E3/0.16 mg/mL tricaine/1% 1-phenyl-2-thiourea (Sigma, USA) and embedded in 0.8% low melt agarose, and then were examined with a Leica TCS-SP5 LSM confocal imaging system. For the results of *in situ* hybridization, Photographs were taken using an Olympus stereomicroscope MVX10. All images of THOC1 immunostaining in mouse were imaged using the Leica SP5 confocal microscope. Statistical analysis was performed using GraphPad Prism software. T-test and one-way analysis of variance (ANOVA) were used, and $P < 0.05$ were considered statistically significant.

Supporting information

S1 Fig. Audiograms of Family SH. Hearing thresholds were averages of both ears. All affected members exhibited symmetric audiometric configuration.
(PDF)

S2 Fig. Quantitative reversed-transcript PCR of 11 protein-coding genes in the critical interval utilizing blood from two family members with (III-10) and without (IV-6) the c.547C>G mutation. Relative expression level is shown as the ratios of that of the affected individual III-10 over the unaffected individual IV-6. None of the 11 genes show significant (P>0.05, t-test) differential expression in the affected individual in comparison with that of the internal control gene (*GAPDH*).
(PDF)

S3 Fig. Reversed-transcript PCR of exons 4–10 of *THOC1* in individuals III-10 and IV-6.
(a) Primer design that amplifies multiple exons (4–10) containing and flanking the c.547C>G mutation (red dash) in exon 7. (b) No differential mRNA expression or alternatively spliced transcript can be detected in the affected individual III-10. (c) Sequencing results of the amplicons.
(PDF)

S4 Fig. Multiple sequence alignment analysis of vertebrate THOC1.
(PDF)

S5 Fig. The validation of monoclonal Anti-THOC1 antibody. (a) Western blot analysis of THOC1 expression in 293t cells and THOC1 knockout 293t cells. (b) Realtime PCR analysis of *THOC1* expression in several cell lines.
(PDF)

S6 Fig. The expression of THOC1 in mouse auditory organ. Confocal microscopic imaging analysis of THOC1 antibody staining in P0 mouse. Blue: DAPI staining of the cell nuclei. Red: Myosin 7a staining marking hair cells. Green: THOC1 antibody staining. Bars, 40 μm.
(PDF)

S7 Fig. *Thoc1* gene knockout using CRISPR/Cas9 system. (a) The targeting sites of gRNAs. (b) Mutation pattern of gRNA1/gRNA2 and cas9 mRNA coinjected embryos. Numbers in the brackets show the number of nucleotides were deleted (-) or inserted (+). Inserted nucleotide

is in red. WT, wild type.
(PDF)

S8 Fig. *Thoc1* knockout caused the reduction of neuromasts in zebrafish. (a) The fluorescence microscopic imaging analysis of control and thoc1 mutants *Tg(cldnb:lynGFP)* zebrafish embryos at 48 hpf. (b) The neuromasts detected by whole mount *in situ* hybridization analysis of *eya1* at 48 hpf. (c) The fluorescence microscopic imaging analysis of control and thoc1 mutants *Tg(cldnb: lynGFP)* zebrafish embryos at 3 dpf. (d) The statistical analysis of the number of neuromasts at each side of the control (n = 12) and *thoc1* mutant (n = 24) embryo trunk at 48 hpf. t-test, ****$P < 0.0001$. (e) The statistical analysis of the number of neuromasts at each side of the control (n = 12) and *thoc1* mutant (n = 23) embryo trunk at 3 dpf. t-test, ****$P < 0.0001$.
(PDF)

S9 Fig. *Thoc1* deficiency caused hair cell developmental defects in zebrafish. (a) Confocal microscopic imaging analysis the hair cells in otic vesicle of control and *thoc1* mutants *Tg (pou4f3:gap43-GFP)* at 3 dpf. (b) Statistical analysis of the hair cells in otic vesicle of control and *thoc1* mutants. *t*-test, ****, $p < 0.0001$.
(PDF)

S10 Fig. C-startle response in *thoc1* deficient zebrafish larva was significantly lower than that in control zebrafish.
(PDF)

S11 Fig. C-startle response in *thoc1* deficient adult zebrafish was significantly lower than that in control zebrafish.
(PDF)

S12 Fig. The sequence alignment of thoc1 in control morpholino and splicing blocking morpholino injected embryos.
(PDF)

S13 Fig. P53 deficiency partially rescues the hair cell developmental defects in thoc1 morphants. (a) The fluorescence microscopic imaging analysis of control, *p53* knockout (KO), *thoc1* morphants, and *p53* KO+ *thoc1*-MO embryos stained with FM1-43FX at 3 dpf. (b, c) Statistical analysis of the hair cell clusters in trunk and head of control, *p53* knockout (KO), *thoc1* morphants, and *p53* KO+ *thoc1*-MO embryos. One-way ANOVA, ****$P < 0.0001$, **$P < 0.01$. (d) Confocal imaging analysis of the hair cells in control, *p53* knockout (KO), *thoc1* morphants, and *p53* KO+ *thoc1*-MO embryos.
(PDF)

S14 Fig. Fluorescence microscopic imaging analysis of thoc1 knockout Tg(*pou4f3: gap43-GFP*) line at 3 dpf. Arrowheads indicate hair cell clusters.
(PDF)

S1 Table. The critical interval from linage analysis of Family SH.
(PDF)

S2 Table. Candidate pathogenic variants identified by exome sequencing of five members of Family SH.
(PDF)

S1 Data. Logarithm of the odds (LOD) scores of genome-wide linkage analysis for chromosomes.
(PDF)

Author Contributions

Conceptualization: Luping Zhang, Dong Liu.

Data curation: Yu Gao, Ru Zhang, Feifei Sun, Penghui Chen, Tao Yang.

Formal analysis: Yu Gao, Ru Zhang, Feifei Sun, Cheng Cheng, Fuping Qian, Cheng Sun, Tao Yang, Dong Liu.

Funding acquisition: Luping Zhang, Dong Liu.

Investigation: Yu Gao, Cheng Cheng, Fuping Qian, Xuchu Duan, Guanyun Wei, Cheng Sun, Xiuhong Pang.

Methodology: Dong Liu.

Supervision: Renjie Chai, Tao Yang, Hao Wu.

Writing – original draft: Luping Zhang, Yu Gao, Dong Liu.

Writing – review & editing: Tao Yang, Hao Wu, Dong Liu.

References

1. Gates GA, Mills JH. Presbycusis. Lancet. 2005; 366(9491):1111–20. https://doi.org/10.1016/S0140-6736(05)67423-5 PMID: 16182900.

2. Hwang JH, Chen JC, Hsu CJ, Yang WS, Liu TC. Plasma reactive oxygen species levels are correlated with severity of age-related hearing impairment in humans. Neurobiol Aging. 2012; 33(9):1920–6. https://doi.org/10.1016/j.neurobiolaging.2011.10.012 PMID: 22133279.

3. Jiang H, Talaska AE, Schacht J, Sha SH. Oxidative imbalance in the aging inner ear. Neurobiol Aging. 2007; 28(10):1605–12. https://doi.org/10.1016/j.neurobiolaging.2006.06.025 PMID: 16920227; PubMed Central PMCID: PMC2453750.

4. Sergeyenko Y, Lall K, Liberman MC, Kujawa SG. Age-related cochlear synaptopathy: an early-onset contributor to auditory functional decline. J Neurosci. 2013; 33(34):13686–94. https://doi.org/10.1523/JNEUROSCI.1783-13.2013 PMID: 23966690; PubMed Central PMCID: PMC3755715.

5. Viana LM, O'Malley JT, Burgess BJ, Jones DD, Oliveira CA, Santos F, et al. Cochlear neuropathy in human presbycusis: Confocal analysis of hidden hearing loss in post-mortem tissue. Hear Res. 2015; 327:78–88. https://doi.org/10.1016/j.heares.2015.04.014 PMID: 26002688; PubMed Central PMCID: PMC4554812.

6. Kwan T, White PM, Segil N. Development and regeneration of the inner ear. Ann N Y Acad Sci. 2009; 1170:28–33. https://doi.org/10.1111/j.1749-6632.2009.04484.x PMID: 19686102.

7. Yamasoba T, Lin FR, Someya S, Kashio A, Sakamoto T, Kondo K. Current concepts in age-related hearing loss: epidemiology and mechanistic pathways. Hear Res. 2013; 303:30–8. https://doi.org/10.1016/j.heares.2013.01.021 PMID: 23422312; PubMed Central PMCID: PMC3723756.

8. Sha SH, Chen FQ, Schacht J. Activation of cell death pathways in the inner ear of the aging CBA/J mouse. Hear Res. 2009; 254(1–2):92–9. https://doi.org/10.1016/j.heares.2009.04.019 PMID: 19422898; PubMed Central PMCID: PMC2749985.

9. Someya S, Xu J, Kondo K, Ding D, Salvi RJ, Yamasoba T, et al. Age-related hearing loss in C57BL/6J mice is mediated by Bak-dependent mitochondrial apoptosis. Proc Natl Acad Sci U S A. 2009; 106 (46):19432–7. https://doi.org/10.1073/pnas.0908786106 PMID: 19901338; PubMed Central PMCID: PMC2780799.

10. Fransen E, Bonneux S, Corneveaux JJ, Schrauwen I, Di Berardino F, White CH, et al. Genome-wide association analysis demonstrates the highly polygenic character of age-related hearing impairment. Eur J Hum Genet. 2015; 23(1):110–5. https://doi.org/10.1038/ejhg.2014.56 PMID: 24939585; PubMed Central PMCID: PMC4266741.

11. Friedman RA, Van Laer L, Huentelman MJ, Sheth SS, Van Eyken E, Corneveaux JJ, et al. GRM7 variants confer susceptibility to age-related hearing impairment. Hum Mol Genet. 2009; 18(4):785–96. https://doi.org/10.1093/hmg/ddn402 PMID: 19047183; PubMed Central PMCID: PMC2638831.

12. Van Laer L, Huyghe JR, Hannula S, Van Eyken E, Stephan DA, Maki-Torkko E, et al. A genome-wide association study for age-related hearing impairment in the Saami. Eur J Hum Genet. 2010; 18(6):685–93. https://doi.org/10.1038/ejhg.2009.234 PMID: 20068591; PubMed Central PMCID: PMC2987344.

13. Dror AA, Avraham KB. Hearing impairment: a panoply of genes and functions. Neuron. 2010; 68 (2):293–308. https://doi.org/10.1016/j.neuron.2010.10.011 PMID: 20955936.

14. Cheng J, Zhu Y, He S, Lu Y, Chen J, Han B, et al. Functional mutation of SMAC/DIABLO, encoding a mitochondrial proapoptotic protein, causes human progressive hearing loss DFNA64. Am J Hum Genet. 2011; 89(1):56–66. https://doi.org/10.1016/j.ajhg.2011.05.027 PMID: 21722859; PubMed Central PMCID: PMC3135809.

15. Walsh T, Pierce SB, Lenz DR, Brownstein Z, Dagan-Rosenfeld O, Shahin H, et al. Genomic duplication and overexpression of TJP2/ZO-2 leads to altered expression of apoptosis genes in progressive non-syndromic hearing loss DFNA51. Am J Hum Genet. 2010; 87(1):101–9. https://doi.org/10.1016/j.ajhg.2010.05.011 PMID: 20602916; PubMed Central PMCID: PMC2896780.

16. Li Y, Wang X, Zhang X, Goodrich DW. Human hHpr1/p84/Thoc1 regulates transcriptional elongation and physically links RNA polymerase II and RNA processing factors. Mol Cell Biol. 2005; 25(10):4023–33. https://doi.org/10.1128/MCB.25.10.4023-4033.2005 PMID: 15870275; PubMed Central PMCID: PMC1087710.

17. Heath CG, Viphakone N, Wilson SA. The role of TREX in gene expression and disease. Biochem J. 2016; 473(19):2911–35. https://doi.org/10.1042/BCJ20160010 PMID: 27679854; PubMed Central PMCID: PMC5095910.

18. Wang X, Chinnam M, Wang J, Wang Y, Zhang X, Marcon E, et al. Thoc1 deficiency compromises gene expression necessary for normal testis development in the mouse. Mol Cell Biol. 2009; 29(10):2794–803. https://doi.org/10.1128/MCB.01633-08 PMID: 19307311; PubMed Central PMCID: PMC2682050.

19. Wang X, Li Y, Zhang X, Goodrich DW. An allelic series for studying the mouse Thoc1 gene. Genesis. 2007; 45(1):32–7. https://doi.org/10.1002/dvg.20262 PMID: 17211872; PubMed Central PMCID: PMC2799240.

20. Xiao T, Roeser T, Staub W, Baier H. A GFP-based genetic screen reveals mutations that disrupt the architecture of the zebrafish retinotectal projection. Development. 2005; 132(13):2955–67. https://doi.org/10.1242/dev.01861 PMID: 15930106.

21. He Y, Lu X, Qian F, Liu D, Chai R, Li H. Insm1a Is Required for Zebrafish Posterior Lateral Line Development. Frontiers in molecular neuroscience. 2017; 10:241. https://doi.org/10.3389/fnmol.2017.00241 PMID: 28824372; PubMed Central PMCID: PMC5539400.

22. Gorczyca W, Traganos F, Jesionowska H, Darzynkiewicz Z. Presence of DNA strand breaks and increased sensitivity of DNA in situ to denaturation in abnormal human sperm cells: analogy to apoptosis of somatic cells. Exp Cell Res. 1993; 207(1):202–5. Epub 1993/07/01. https://doi.org/10.1006/excr.1993.1182 PMID: 8391465.

23. Lozano GM, Bejarano I, Espino J, Gonzalez D, Ortiz A, Garcia JF, et al. Relationship between caspase activity and apoptotic markers in human sperm in response to hydrogen peroxide and progesterone. J Reprod Dev. 2009; 55(6):615–21. Epub 2009/09/08. https://doi.org/10.1262/jrd.20250 PMID: 19734695.

24. Kanehisa M, Goto S. KEGG: kyoto encyclopedia of genes and genomes. Nucleic Acids Res. 2000; 28 (1):27–30. Epub 1999/12/11. https://doi.org/10.1093/nar/28.1.27 PMID: 10592173; PubMed Central PMCID: PMC102409.

25. Haupt S, Berger M, Goldberg Z, Haupt Y. Apoptosis—the p53 network. J Cell Sci. 2003; 116(Pt 20):4077–85. Epub 2003/09/16. https://doi.org/10.1242/jcs.00739 PMID: 12972501.

26. Murphy KM, Ranganathan V, Farnsworth ML, Kavallaris M, Lock RB. Bcl-2 inhibits Bax translocation from cytosol to mitochondria during drug-induced apoptosis of human tumor cells. Cell Death Differ. 2000; 7(1):102–11. Epub 2000/03/14. https://doi.org/10.1038/sj.cdd.4400597 PMID: 10713725.

27. Porter AG, Janicke RU. Emerging roles of caspase-3 in apoptosis. Cell Death Differ. 1999; 6(2):99–104. Epub 1999/04/14. https://doi.org/10.1038/sj.cdd.4400476 PMID: 10200555.

28. Li P, Nijhawan D, Budihardjo I, Srinivasula SM, Ahmad M, Alnemri ES, et al. Cytochrome c and dATP-dependent formation of Apaf-1/caspase-9 complex initiates an apoptotic protease cascade. Cell. 1997; 91(4):479–89. Epub 1997/12/09. https://doi.org/10.1016/s0092-8674(00)80434-1 PMID: 9390557.

29. Chinnam M, Wang X, Zhang X, Goodrich DW. Evaluating Effects of Hypomorphic Thoc1 Alleles on Embryonic Development in Rb1 Null Mice. Mol Cell Biol. 2016; 36(11):1621–7. https://doi.org/10.1128/MCB.01003-15 PMID: 27001308; PubMed Central PMCID: PMC4959316.

30. Dominguez-Sanchez MS, Saez C, Japon MA, Aguilera A, Luna R. Differential expression of THOC1 and ALY mRNP biogenesis/export factors in human cancers. BMC Cancer. 2011; 11:77. https://doi.org/10.1186/1471-2407-11-77 PMID: 21329510; PubMed Central PMCID: PMC3050854.

31. Guo S, Hakimi MA, Baillat D, Chen X, Farber MJ, Klein-Szanto AJ, et al. Linking transcriptional elongation and messenger RNA export to metastatic breast cancers. Cancer Res. 2005; 65(8):3011–6. https://doi.org/10.1158/0008-5472.CAN-04-3624 PMID: 15833825.

32. Li Y, Lin AW, Zhang X, Wang Y, Wang X, Goodrich DW. Cancer cells and normal cells differ in their requirements for Thoc1. Cancer Res. 2007; 67(14):6657–64. https://doi.org/10.1158/0008-5472.CAN-06-3234 PMID: 17638875; PubMed Central PMCID: PMC2804983.

33. Xiong H, Pang J, Yang H, Dai M, Liu Y, Ou Y, et al. Activation of miR-34a/SIRT1/p53 signaling contributes to cochlear hair cell apoptosis: implications for age-related hearing loss. Neurobiol Aging. 2015; 36 (4):1692–701. https://doi.org/10.1016/j.neurobiolaging.2014.12.034 PMID: 25638533.

34. Fox CS, Coady S, Sorlie PD, Levy D, Meigs JB, D'Agostino RB Sr., et al. Trends in cardiovascular complications of diabetes. JAMA. 2004; 292(20):2495–9. Epub 2004/11/25. https://doi.org/10.1001/jama.292.20.2495 PMID: 15562129.

35. Gong J, Wang X, Zhu C, Dong X, Zhang Q, Wang X, et al. Insm1a Regulates Motor Neuron Development in Zebrafish. Front Mol Neurosci. 2017; 10:274. https://doi.org/10.3389/fnmol.2017.00274 PMID: 28894416; PubMed Central PMCID: PMC5581358.

36. Wang X, Ling CC, Li L, Qin Y, Qi J, Liu X, et al. MicroRNA-10a/10b represses a novel target gene mib1 to regulate angiogenesis. Cardiovascular research. 2016; 110(1):140–50. https://doi.org/10.1093/cvr/cvw023 PMID: 26825552.

37. Zhang J, Qi J, Wu S, Peng L, Shi Y, Yang J, et al. Fatty Acid Binding Protein 11a Is Required for Brain Vessel Integrity in Zebrafish. Frontiers in physiology. 2017; 8:214. https://doi.org/10.3389/fphys.2017.00214 PMID: 28443032; PubMed Central PMCID: PMC5387095.

38. Huang Y, Wang X, Xu M, Liu M, Liu D. Nonmuscle myosin II-B (myh10) expression analysis during zebrafish embryonic development. Gene expression patterns: GEP. 2013; 13(7):265–70. Epub 2013/05/15. S1567-133X(13)00043-4 [pii] https://doi.org/10.1016/j.gep.2013.04.005 PMID: 23665442.